Available online at www.sciencedirect.com
ScienceDirect
Journal of Catalysis 253 (2008) 132–138
JOURNAL OF CATALYSIS
www.elsevier.com/locate/jcat

Catalytic reduction of oxygen and hydrogen peroxide by nanoporous gold

Roswitha Zeis [a], Tang Lei [b], Karl Sieradzki [b], Joshua Snyder [a], Jonah Erlebacher [a,*]

[a] *Department of Materials Science and Engineering and Department of Chemical and Biomolecular Engineering, Johns Hopkins University, Baltimore, MD 21218, USA*

[b] *Department of Chemical and Materials Engineering, Arizona State University, Tempe, AZ 85287, USA*

Received 21 August 2007; revised 16 October 2007; accepted 16 October 2007

Available online 26 November 2007

Abstract

Nanoporous gold (NPG) made by dealloying silver/gold alloys is a mesoporous metal combining high surface area and high conductivity. Recently, NPG has been shown to exhibit some of the high catalytic activity previously associated only with supported gold nanoparticles. Here we describe how NPG acts as a catalyst for the oxygen reduction reaction in both gas phase (in fuel cells) and aqueous environments (using rotating disk electrochemistry). NPG was found to reduce oxygen via an effectively 4-four electron route comprised of a first reduction of oxygen to hydrogen peroxide, and then an unusually active further catalytic reduction of hydrogen peroxide to water.

Keywords: Nanoporous gold; Oxygen reduction reaction; Fuel cells

1. Introduction

The catalytic activity of nanostructured gold has been of interest since the discovery by Haruta et al. [1] that gold nanoparticles supported on oxides exhibit remarkable activity for oxidation of CO, remaining highly active even at temperatures below 0 °C. Since that report, many examples of supported nanoparticulate gold catalysis have been reported, including partial oxidation of organic molecules [2,3] and reduction of oxygen to hydrogen peroxide [4–7]. Central to the interest surrounding these results have been the question of whether the gold nanoparticles by themselves are responsible for the catalytic activity through, for instance, a quantum size effect, or whether the electronic–ionic interaction between the particles and the supporting oxide plays a role [8,9].

Recent work suggests a synergy between the oxide and the gold; that is, not only is nanostructured gold by itself quite active (in some case highly active) to a variety of catalytic reactions, but also the presence of nearby reducible oxide may facilitate electron transfer reactions and potentially increase the intrinsic catalytic activity [10]. The primary reason that bulk planar gold is not particularly active catalytically is that the catalytic sites are often crystal surface defect sites, such as step edges. At these sites, gold atoms with lower bond coordination are found, and the presence of dangling bonds may help adsorption of reactants through electronic and/or steric considerations. This observation leads to the hypothesis that gold surfaces roughed artificially (by, e.g., ion beams) should be more active than planar gold, and this observation has been made for the case of CO oxidation in a series of experiments by Yim et al. [11].

If crystalline step edges are helpful for enhancing the catalytic activity of gold, then it seems likely that forms of gold with significant number of step sites should be good catalysts. A useful but relatively unstudied form of gold that likely contains an intrinsically high step density is the mesoporous form typically called "nanoporous gold" (NPG) [12,13]. NPG is made by chemically dealloying silver from silver/gold alloys, resulting in a typical pore size of 10–20 nm and a specific surface area approximately 4 m^2/g, which is high for a precious metal (see Fig. 1). Because NPG may be described as an interconnected, bicontinuous ligament network containing regions of both negative and positive curvature, a high step density is topologically required. This characteristic makes NPG attractive for catalysis studies; it is made even more attractive because

* Corresponding author.
E-mail address: jonah.erlebacher@jhu.edu (J. Erlebacher).

0021-9517/$ – see front matter
doi:10.1016/j.jcat.2007.10.017

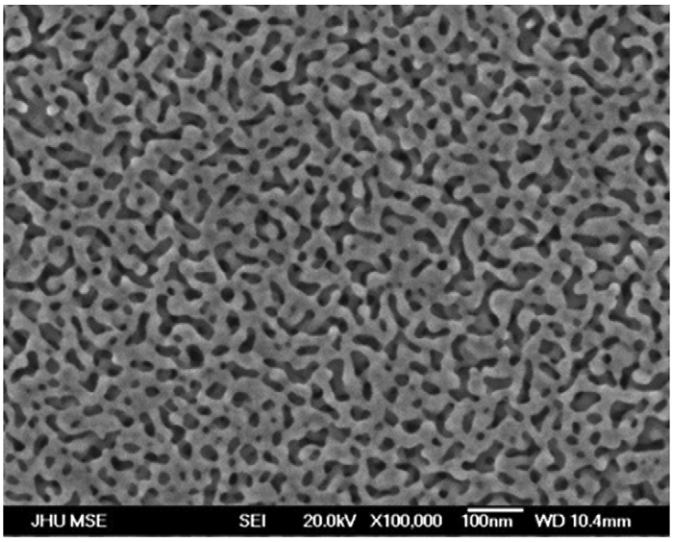

Fig. 1. Scanning electron microscopy (SEM) micrograph of dealloyed nanoporous gold leaf.

it can be easily formed into thin, high-conductivity foils that are easily adapted to electrocatalytic measurements [14].

A few recent studies have addressed the catalytic activity of NPG. Xu et al. [15] and Zielasek et al. [16] have shown that NPG by itself exhibits catalytic oxidation of CO to CO_2. This reaction is also highly active even below room temperature and rivals the activity of supported gold nanoparticles. Zhang et al. [17] showed that NPG is also catalytic toward methanol electrooxidation. They found that the higher the porosity (smaller pore size), the higher the activity. This observation is consistent with step edges being the catalytic sites.

In our previous work, we examined the use of NPG coated with atomically thin epitaxial skins of platinum, and using membrane foils of the Pt-plated NPG material as anode and cathode electrodes in H_2/O_2 proton-exchange membrane (PEM) fuel cells [18]. Pt-NPG works quite well in the fuel cell application, achieving high power densities at very low Pt loads. Driven by the general growing interest in gold catalysis alone, we decided to test the utility of NPG alone as an anode and cathode. NPG was not found to exhibit any activity toward hydrogen oxidation (the anode reaction), but we were surprised to discover that NPG exhibits quite appreciable activity for oxygen reduction. One reason for our surprise was that although oxygen reduction has been seen on gold in alkaline environments—indeed, it is quite efficient in basic media [19]—there has been no evidence of it occurring in acidic environments such as PEM fuel cells. This paper details our subsequent study of oxygen reduction over NPG. Overall, our results are consistent with an oxygen reduction mechanism that proceeds via two separate two electron reductions, and not the high efficiency four-electron oxygen reduction reaction (ORR) exhibited by Pt. The first reduction step, oxygen to hydrogen peroxide, occurs at overpotentials characteristic of bulk gold (but at appreciable rates, adjusting for the enhanced surface area of NPG). The second reduction step, reduction of hydrogen peroxide to water, is catalyzed very efficiently by NPG.

We first describe our characterization of the ORR in the gaseous environment of the PEM fuel cell. We then performed aqueous phase experiments using rotating disk electrochemistry (RDE) and rotating ring disk electrochemistry (RRDE) to determine the reaction pathway for ORR over NPG. We find that an initial reduction of oxygen to hydrogen peroxide step is rate-limiting, because the further reduction of hydrogen peroxide to water is strongly catalyzed by NPG.

2. Experimental

2.1. Membrane electrode fabrication

NPG electrode foils were prepared by dealloying a 12-carat white gold leaf (Monarch; Sepp Leaf Products; 50/50 wt% Au/Ag) by floating it on a bath of concentrated nitric acid (70%, Fisher Scientific) as described in detail previously. This process resulted in an approximate 100-nm-thick freestanding thin film of NPG leaf (NPGL) approximately 80 cm^2 in area. A scanning electron microscopy (SEM) micrograph of the surface of NPGL is shown in Fig. 1. The pore size of NPGL can be increased from 15 to 40 nm by leaving the material for prolonged periods in the acid bath. At ∼15 nm pore sizes, a residual concentration of ∼4% Ag was found using energy-dispersive spectroscopy (EDAX), and this dropped to below the detectable limit of the spectrometer (<0.1%) on coarsening in acid.

Anodes were Pt-plated NPGL (Pt-NPGL), created as described previously. In brief, a conformal skin of platinum was plated on NPGL using a variation of electroless deposition in which the leaf is placed at the interface between a bath containing a platinum salt solution (sodium hexachloroplatinate) and a vapor containing a reducing agent (hydrazine). For all of the experiments discussed, the Pt loading of the anode was approximately 0.05 mg cm^{-2}, as determined by precision weight measurements of large-area (50 cm^2) samples before and after platinum deposition. Cathodes were as-prepared NPGL, with no platinum deposition.

To make the final MEA, the cathode (NPGL) and anode (Pt-NPGL) electrodes were floated on water baths and then lifted onto 2.2-cm-diameter mica disks and dried. These disks served as stamps to print them simultaneously onto the two sides of a Nafion 113.5 membrane. In this printing process, the Nafion membrane was moisturized, placed between the two mica disks carrying the electrode materials, and then hot-pressed at a temperature of about 70 °C and a pressure of about 2000 psi for approximately 5 min, as described previously.

2.2. Fuel cell testing

As-prepared MEAs were sandwiched between two pieces hydrophobic carbon cloth, which served as a gas-diffusion layer (GDL, EKT 2051), and tested in 10-cm^2 cells with stainless steel serpentine flow fields. Silicone gaskets were used to seal the cell. Hydrogen and oxygen were humidified using temperature-controlled bubble humidifiers to 100% relative humidity, and fed into the fuel cell system. The typical operating pressure and gas flow rate were 35 psi and 1 sccm, respectively.

The voltage-current curves were measured at room temperature using an electronic load (Array 3710A).

To characterize the electrode surface electrochemically, hydrogen adsorption was measured by cyclic voltammetry (CV) using a Gamry Z750 potentiostat. In the CV experiments, we used a standard setup for these measurements in which the flow of oxygen was replaced by nitrogen. For platinum-based catalysts, the active surface area usually is determined by charge integration of the monolayer hydrogen adsorption peak. Here the cathode contained no Pt, and we saw no hydrogen adsorption. Therefore, the relative active surface area of the gold was determined by charge integration of the oxide reduction peak obtained from the cyclic voltammogram. Cyclic voltammograms were obtained at a scan rate of 550 mV s^{-1}.

2.3. RRDE and RDE electrochemistry

For all RRDE and RDE experiments, the working electrode consisted of a disk (bare gold or NPG [50/50 wt% Au/Ag, geometric area 0.28 cm^2]), and the ring electrode was Pt, sealed in a polytetrafluroethylene holder. The bulk planar gold electrode was polished with a 0.05-μm alumina suspension on a polishing cloth and then cleaned ultrasonically in deionized water (Millipore). For the NPG electrodes, we prepared a rod (0.4 cm diameter) of silver/gold alloy ($Au_{35}Ag_{65}$) that was cut into approximately 0.5-mm-thick disks. These disks were polished to a mirror finish, and then annealed for 2 h at 800 °C to relieve internal stresses. We then dealloyed the samples by applying a few drops of concentrated nitric acid on their surfaces. Dealloying was allowed to proceed for 2 min, after which the sample was thoroughly rinsed with deionized water. This produced a porous layer at least 40 nm thick.

The relative roughness of planar gold electrodes to NPG was found by oxidation and stripping cycles of each material in 0.25 M nitric acid, integrating the stripping charge. The relative roughness between the 5-min dealloyed NPG (a 100-nm-thick porous layer) and planar gold was 12.6. Thus, the 40-nm-thick NPG used in the rotating disk electrodes thus had a relative roughness of approximately 5.

Both RRDE and RDE experiments used an AFASR rotator (Pine Instruments), a saturated calomel electrode (SCE) as reference electrode, and a Pt wire counter electrode. For the RRDE experiments, an AFM TI34 rotating ring disk electrode (Pine Instruments) using a Pt ring electrode was added to the setup. All potentials reported are relative to SCE. A salt bridge was placed between the reference electrode and the cell, preventing electrolyte contamination by Cl^-. The disk and ring potentials were applied with an AFRDE5 Bi-Potentiostat (Pine Instruments).

The study of oxygen reduction kinetics on NPG used an RRDE setup with an electrolyte of 0.5 M H_2SO_4 saturated with pure oxygen (Air Products). For the hydrogen peroxide reduction experiments, the electrolyte was a 0.5 M H_2SO_4 solution containing 1 mM H_2O_2 (Fluka), deaerated with argon gas (Air Products). The ring electrode potential, where the peroxide oxidation occurred, was kept at 1.1 V, whereas the disk electrode potential was between −0.2 and 0.4 V, with a scan rate of 50 mV s^{-1}. All voltammograms were recorded at room temperature.

3. Results and discussion

3.1. Gas-phase oxygen reduction by NPG in a PEM fuel cell environment

A typical polarization curve of a PEM fuel cell using a NPG cathode and Pt-NPG anode is presented in Fig. 2. The current density was much lower than typical results from conventional PEM fuel cells using Pt-based materials for both cathode and anode [20], because oxygen reduction occurs more slowly on gold (NPG in this case) than on Pt. The potential dropped quickly as the current increased, indicating a large activation loss. Nevertheless, at room temperature, a current density of up to 125 mA/cm^2 at 140 mV could be obtained. Particularly interesting (and surprising to some extent) is the finding that the open circuit potential was as high as 850 mV, a value not much lower than the open circuit potential of PEM fuel cells with Pt catalyst cathodes.

We characterized the NPG cathode electrochemically by in situ cyclic voltammetry (CV) of NPG cathodes with varying pore size. We found no significant variation in the polarization behavior under H_2/O_2 conditions as the pore size was increased from ∼15 to ∼40 nm, although cyclic voltammetry under H_2/N_2 conditions showed a marked change. Fig. 3 shows the CV response of NPG in the cathode under H_2/N_2. These gas-phase results are basically the same as the typical response of gold electrodes in acid solutions; namely, we found oxidation and reduction waves representing the formation and reduction of a surface gold oxide. The surface area is a function of the pore size; as pore size increased, the peaks of the oxidation and

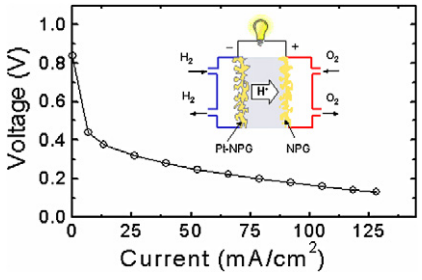

Fig. 2. Voltage–current polarization of a NPG MEA (cathode: NPG and anode: Pt-NPG) at room temperature.

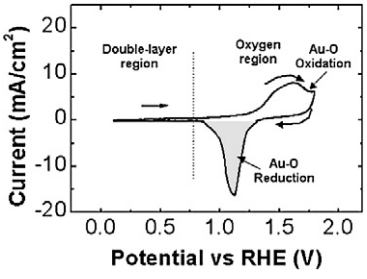

Fig. 3. Cyclic voltammogram for NPG electrode in the fuel cell environment at a scan rate of 550 mV/s.

reduction waves decreased. For the typical pore size of 15 nm in NPGL (the pore size in dealloyed nitric acid), we know from BET measurements [21] that the roughness factor of NPGL is approximately 10. This served to roughly calibrate the roughness factor for the larger pore sizes. Ultimately, we probed NPG with roughness factors of 2–10 over planar gold. Within this range, the polarization behavior remained unchanged, which led to a hypothesis that the catalytic sites are likely not those parts of the crystalline surface that contribute to the geometric area (i.e., terraces), but likely step edges whose surface density may not change significantly with pore size and/or are so active that reactions at these sites are not rate-limiting.

Cathodic oxygen reduction is a multielectron reaction often associated with the formation of reaction intermediates. Several reaction mechanisms have been suggested; the most common being those originally proposed by Damjanovic et al. [22]:

(i) A direct four electron reduction to H_2O:

$$O_2 + 4H^+ + 4e^- \rightarrow 2H_2O, \qquad E_0 = 1.229 \text{ V vs RHE.}$$

This mechanism occurs predominantly on Pt.

(ii) A two-electron pathway involving reduction to hydrogen peroxide commonly seem on bulk gold:

$$O_2 + 2H^+ + 2e^- \rightarrow H_2O_2, \qquad E_0 = 0.67 \text{ V vs RHE.}$$

(iii) A four-electron process reduction that occurs in two steps:

$$O_2 + 2H^+ + 2e^- \rightarrow H_2O_2$$

and

$$H_2O_2 + 2H^+ + 2e^- \rightarrow 2H_2O.$$

Here oxygen is first reduced to hydrogen peroxide, and then further reduced to water.

We rule out pathway (ii) as the only ORR pathway seen on NPG, because this process alone would not be able to produce an open circuit potential >0.67 V. The high open-circuit potential of ∼0.85 V strongly suggests a four-electron process, either directly [pathway (i)] or indirectly [pathway (iii)]. Furthermore, if pathway (ii) were operative, we should be able to detect peroxide in the output reactant stream of our cell (approximately 0.32 g/h at a current of 0.5 A). Toward this end, we inserted sensitive peroxide test sticks (Quantofix Peroxide 100, Sigma–Aldrich) into the output of the fuel cell to test for hydrogen peroxide, but found none.

3.2. Aqueous-phase oxygen reduction on NPG

Based on the relatively low currents and voltages observed in the polarization behavior, we thought that pathway (iii) was the most likely candidate for ORR on NPG. This reaction pathway has been proposed for ORR on gold nanoparticles electrodeposited on gold electrodes, a system that also exhibits high activity toward hydrogen peroxide reduction [23]. RDE in aqueous solution allows separation of the partial reaction paths in (iii), measuring the Tafel slope associated with each path, and testing whether the ORR seen in the PEM fuel cell environment is actually the two-step, four-electron process.

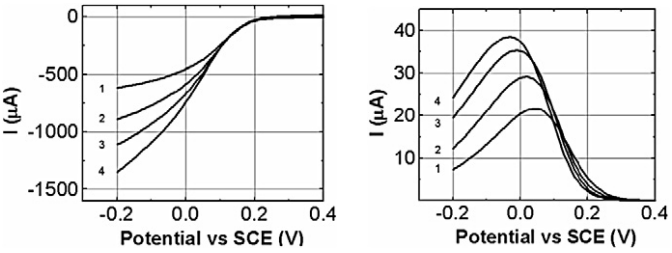

Fig. 4. Disk (a) and ring currents (b) during oxygen reduction on NPG at various rotation rates (1) 400, (2) 900, (3) 1600, and (4) 2500 rpm.

We used RRDE to determine the ORR pathway on NPG. This experiment allowed us to examine the catalytic activity of NPG in a cleaner and better-controlled environment than the fuel cell setup, because we wanted to rule out the presence of impurities that might contribute to and affect experimental results. Most importantly, the rotating ring disk is an excellent tool for detecting hydrogen peroxide. Any hydrogen peroxide generated at the disk (working) electrode is swept outward under convection caused by rotation and can be detected electrochemically at the ring. The ring is kept at high positive potential (1.1 V vs SCE), and thus all of the peroxide that reaches the ring electrode is oxidized. Consequently, the current on the ring is a direct measurement of the presence of hydrogen peroxide alone, whereas the disk current records a sum of the oxygen reduction currents of both peroxide and water.

Fig. 4 shows the disk (a) and ring (b) currents with various rotation rates for oxygen reduction on NPG. These results are similar to oxygen reduction rates on Au single crystals in acidic media reported by Adzic et al. [24]. Each curve is an average of forward and backward scans to eliminate the contribution of double-layer charging. For the disk current, no well-defined current plateau is present at potentials before hydrogen evolution. This is due to the mixed kinetic-diffusion control of the reaction. The onset of the ORR is at approximately 0.2 V. The maximum ring current occurs at approximately 0 V, reaching levels of 5–6% of the disk current (uncorrected for the ring collection efficiency). The relatively large ratio of ring to disk current further rules out the direct four-electron transfer process as the ORR pathway on NPG and again points to pathway (iii), the indirect four-electron transfer process in two separate steps.

A more detailed analysis of the ring current, known as the Koutecky–Levich analysis, confirmed our findings and clarified the rate-limiting step for oxygen reduction on NPG. The graph of inverse current (I^{-1}) versus the inverse square root of the rotation range ($\omega^{-0.5}$), a Koutecky–Levich plot, is presented in Fig. 5. A linear fit for each potential intercepts the vertical axis at the kinetic current I_{kin}, which is used to assess the catalytic reaction kinetics without the complications of diffusional processes. In the small-current regime, I_{kin} grows exponentially with the applied potential, exhibiting Tafel behavior. From the semilog plot shown in Fig. 8, we obtain a Tafel slope of 120 mV per decade. This is in good agreement with the values reported in the literature for oxygen reduction on planar gold electrodes in acid solution, with reported Tafel slopes in the range of 102–120 mV per decade [25,26]. This result strongly suggests that if

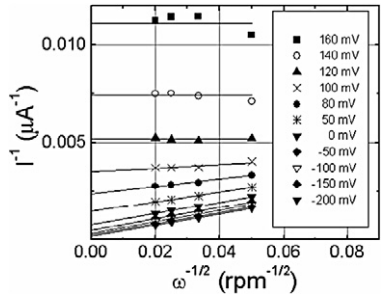

Fig. 5. Koutecky–Levich plot for oxygen reduction on NPG at various electrode potentials.

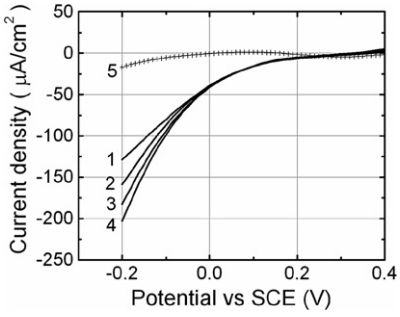

Fig. 6. Disk currents during peroxide reduction on and NPG at various rotation rates (1) 400, (2) 900, (3) 1600, and (4) 2500 rpm. Curve (5) is the (negligible) disk current during the peroxide reduction on bulk, planar gold at $\omega =$ 1600 rpm. Note that disk current are given as per real surface area, and not per projected geometric area.

reaction (iii) is operative with NPG, then the rate-determining step is the first electron transfer reaction. For completeness, we repeated the RRDE experiments using bulk planar gold as a working electrode and obtained similar current–voltage characteristics for the disk and ring as seen with NPG, except that the onset of the ORR was shifted toward 0.1 V. Once more, we extrapolated from the Koutecky–Levich plot a Tafel slope for the ORR on bulk gold and obtained the same value of 120 mV per decade (see Fig. 8).

3.3. Reduction of hydrogen peroxide by NPG

In the RRDE, the hydrogen peroxide generated at the disk is swept away and oxidized at Pt ring. Some of the peroxide, however, might be reduced at the electrode or spontaneously reduced as it is swept to the ring. This prevents us from independently observing the reduction of hydrogen peroxide to water. To prove that NPG, in contrast to bulk planar gold, promotes the reduction of hydrogen peroxide to water, we performed RDEs in a deaerated H_2SO_4 electrolyte containing hydrogen peroxide, directly measuring the peroxide reduction current. Fig. 6 shows the current–potential curves for hydrogen peroxide reduction on NPG, along with a representative curve on bare gold recorded at 1600 rpm. To make the different between bulk gold and NPG clear, we plotted current densities against real surface area. For the case of bulk planar gold, the measured disk currents were insignificant, lying within the noise range of the instrument (<10 μA). Using NPG with the same peroxide-containing solution, we obtained a clear disk signal

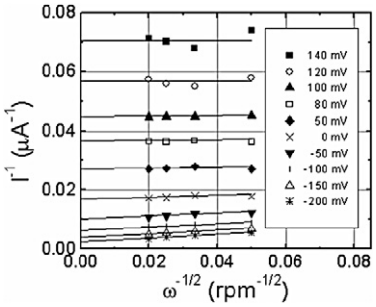

Fig. 7. Koutecky–Levich plot of peroxide reduction on NPG.

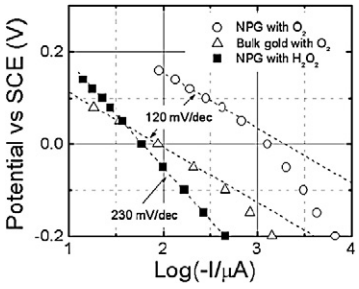

Fig. 8. Tafel plots for peroxide reduction on NPG, oxygen reduction on NPG oxygen reduction on bare gold.

that increased with the rotation speed, demonstrating that the measurement is not an artifact. We find that the onset of the hydrogen peroxide reduction reaction over NPG occurred at approximately 0.2 V. Based on these experimental results, we were able to perform a Koutecky–Levich analysis (Fig. 7) and extrapolated a Tafel slope of 230 mV per decade (Fig. 8) for the hydrogen peroxide reduction reaction on NPG.

Taken together, our results suggest that ORR on NPG proceeds by a rate-limiting reduction of oxygen to hydrogen peroxide, followed by a rapid reduction of hydrogen peroxide to water. A very simple test demonstrates this conclusion very effectively; namely, when a water droplet that contains 5% of hydrogen peroxide is placed onto a NPG sample, gas bubbles are formed instantly on the sample surface in a very vigorous reaction that quickly consumes the hydrogen peroxide. When we repeated the same experiment for a piece of bulk gold as well as for carbon black, we found no gas bubble formation.

3.4. Reaction sites on NPG

The results presented here, as well as a small but growing body of literature evidence, demonstrate that NPG is highly catalytic to some reactions that do not appear to proceed on bulk planar gold. More quantitatively, the reaction currents (associated with, e.g., hydrogen peroxide reduction) are many times greater than the roughness factor (<10) between the NPG samples used here and bulk planar, gold samples. What might be special about NPG that leads to its catalytic properties?

Three structural properties might be involved. The first property is that microscopically, NPG is essentially a porous single crystal; that is, the length scale of porosity is a few orders of magnitude smaller than the grain size (15 nm vs 10 μm). Therefore, in principle, the high curvature ligaments might expose

various facet orientations to the environment, and perhaps our results can be explained in terms of a particular catalytic activity of a particular facet. In principle, the facet orientation distribution may be measured by Pb underpotential deposition (UPD), observing that particular facet orientations exhibit distinct UPD signatures. This was recently done for nanoparticles [27], but such experiments are hampered in NPG by the requirement of Pb diffusion into the nanopores to complete the monolayer. In our experiments, this diffusion limitation effect tends to smear the UPD peaks and make detailed analysis of this kind difficult, if not impossible. In any case, the small scale of the ligaments also makes surface energy effects very prominent, and simulation and electron microscopy evidence demonstrates that NPG is essentially (111) microfaceted [28]. Because no remarkable catalytic activity on Au(111) toward hydrogen peroxide reduction has been seen, we think it unlikely that facet orientation played a significant role here.

The second structural property of NPG that may affect catalytic activity is a thermodynamic size effect (i.e., surface stress), which should lead to bulk compression of material and a reduction in lattice parameters. Such an effect might play an important role in very small pore NPG created by electrochemical dealloying under potential control [29,30], but the samples used in this study were created by dealloying under free corrosion. Either way, X-ray diffraction of NPG formed under potential control showed insignificant changes in the lattice parameter ($< \sim 0.2\%$) compared with bulk gold [31].

The third structural property of NPG that may be involved in its unusual catalytic activity is the presence of a potentially high step density (or, generally, low-coordination surface atoms [32]). Unfortunately, although simulations of NPG formation show that the process of porosity evolution is locally a layer-by-layer stripping process leading to a large step density, no experiments directly testing this surface structural model have been reported. Some indirect evidence exists, however; for instance, Zhang et al. recently reported that with a small amount of galvanic displacement of Au by Pt from the surface of NPG, the thermal stability of NPG is greatly increased. Because galvanic displacement is directly related to the ease with which an atom can desorb from a surface, the likely spots for galvanic displacement in the Au/Pt system are low-coordination step edges. Moreover, in situ SEM of the early stages of roughness evolution during dealloying has shown that the surface retains a terrace/step structure [33].

If, as we hypothesize, step edges are the catalytic sites for hydrogen peroxide reduction, then our observation that the polarization behavior in the fuel cell is independent of pore size may seem odd. However, the range of specific surface areas tested was not large, and the rate-limiting step was shown to be the reduction of oxygen to hydrogen peroxide. Because this rate-limiting reaction occurs on planar gold as well as on NPG, it is a reaction that presumably also can proceed at terrace sites. At this point, however, the step-edge site reaction for hydrogen peroxide reduction is a hypothesis that might be tested by examining the catalytic activity of planar gold surfaces artificially roughened by ion beams or electrochemical oxidation/reduction cycles.

4. Conclusions

NPG has been found to be an effective catalyst for the reduction of hydrogen peroxide to water. The reaction efficiency is sufficiently high to allow use of the material as a cathode for oxygen reduction in hydrogen PEM fuel cells, although the overall efficiency in this context is still far less efficient than that of Pt. Generally, however, it is important to note how that the pace of discovery of the number of reactions for which NPG by itself is a good catalyst is rapidly increasing, and many different systems in which NPG may be the superior catalyst remain to be examined.

Our results here are consistent with our overall hypothesis that the central difference between NPG and bulk gold is due to the increased density of step edges in NPG overall bulk gold. This should be critically examined in future work.

Finally, NPG on oxide supports have been proposed as a catalyst for hydrogen peroxide production [34]. In principle, by running NPG electrochemically in the fuel cell environment to reduce oxygen, hydrogen peroxide will be produced if the reaction is fast enough. However, we have demonstrated that the secondary reaction of peroxide reduction to water is so efficient that it tends to dominate the overall reaction, even at room temperature. As a result, our results for ORR on NPG are temperature-independent over the range of temperatures that we have examined (roughly 23–70 °C), so we believe it unlikely that in the traditional PEM configuration that NPG alone can be used to make hydrogen peroxide. Nonetheless, we leave open the possibility that development of an appropriate electrolyte at subzero or near-zero temperatures (following, e.g., the strategy of Hutchings), the fabrication of an appropriate NPG/oxide composite that enhances hydrogen peroxide formation and slows its further reduction, or appropriate surfactants that selectively passivate step edges reducing their catalytic activity, are paths by which NPG may be modified to serve as a good catalyst for hydrogen peroxide production.

Acknowledgments

We gratefully acknowledge support for this work from the U.S. Department of Energy, Office of Basic Energy Sciences under grant DE-FG02-05ER15727.

References

[1] M. Haruta, T. Kobayashi, H. Sano, N. Yamada, Chem. Lett. 4 (1987) 405.
[2] M. Hughes, Y.-J. Xu, P. Jenkins, P. McMorn, P. Landon, D. Enache, A. Carley, G.A. Attard, G.J. Hutchings, F. King, E.H. Stitt, P. Johnston, K. Griffin, C.J. Kiely, Nature 437 (2005) 1132.
[3] A. Corma, M. Domine, Chem. Commun. (2005) 4042.
[4] G. Li, J. Edwards, A. Carley, G. Hutchings, Catal. Today 114 (2006) 369.
[5] G. Li, J. Edwards, A. Carley, G. Hutchings, Catal. Commun. 8 (2007) 247.
[6] M. El-Deab, T. Ohsaka, Electrochem. Acta 52 (2007) 2166.
[7] C. Raj, A. Abdelrahman, T. Ohsaka, Electrochem. Commum. 7 (2005) 888.
[8] D. Thompson, Top. Catal. 38 (2006) 231.
[9] G. Hutchings, Catal. Today 100 (2005) 55.
[10] N. Lopez, T.V.W. Janssens, B.S. Clausen, Y. Xu, M. Mavrikakis, T. Bligaard, J.K. Norskov, J. Catal. 223 (2004) 232.

[11] W.-L. Yim, T. Nowitzki, M. Necke, H. Schnars, P. Nickut, J. Biener, M.M. Biener, V. Zielasek, K. Al-Shamery, T. Kluner, M. Baumer, J. Phys. Chem. C 111 (2007) 445.
[12] J. Erlebacher, M.J. Aziz, A. Karma, N. Dimitrov, K. Sieradzki, Nature 410 (2001) 450.
[13] Y. Ding, Y.-J. Kim, J. Erlebacher, Adv. Mater. 16 (2004) 1897.
[14] Y. Ding, M. Chen, J. Erlebacher, J. Am. Chem. Soc. 126 (2004) 6876.
[15] C. Xu, et al., J. Am. Chem. Soc. 129 (2007) 42.
[16] V. Zielasek, B. Jürgens, C. Schulz, J. Biener, M.M. Biener, A.V. Hamza, M. Bäumer, Angew. Chem. Int. Ed. 45 (2006) 8241.
[17] J. Zhang, P. Liu, H. Ma, Y. Ding, J. Phys. Chem. C 111 (2007) 10382.
[18] R. Zeis, A. Mathur, G. Fritz, J. Lee, J. Erlebacher, J. Power Sources 165 (2007) 65.
[19] R. Adzic, in: J. Lipkowski, P.N. Ross (Eds.), Electrocatalysis, Wiley–VCH, New York, 1998, p. 197.
[20] J. Lipkowski, P.N. Ross, Electrocatalysis, Wiley–VCH, New York, 1998.
[21] C. Ji, P. Searson, J. Phys. Chem. B 107 (2003) 4494.
[22] A. Damjnovic, M. Genshaw, J. Bockris, J. Phys. Chem. 45 (1966) 3761.
[23] M. El-Deab, T. Ohsaka, Electrochem. Commun. 4 (2002) 288.
[24] R. Adzic, S. Strbac, N. Anastasijevic, Mater. Chem. Phys. 22 (1989) 349.
[25] J. Maruyama, M. Inaba, Z. Ogumi, J. Electroanal. Chem. 458 (1989) 175.
[26] A. Sarapuu, K. Tammeveski, T. Tenno, V. Sammelselg, K. Konturri, D. Schiffrin, Electrochem. Commun. 3 (2001) 446.
[27] J. Hernandez, J. Solla-Gullon, E. Herrero, J. Electroanal. Chem. 574 (2004) 185.
[28] J. Erlebacher, J. Electrochem. Soc. 151 (2004) C614.
[29] S. Parida, D. Kramer, C.A. Volkert, H. Rösner, J. Erlebacher, J. Weissmüller, Phys. Rev. Lett. 97 (2006) 035504.
[30] D. Crowson, D. Farkas, S.G. Corcoran, Scripta Mater. 56 (2007) 919.
[31] Y. Ding, Ph.D. thesis, Johns Hopkins University, 2004.
[32] T.V.W. Jansenns, A. Carlsson, A. Puig-Molina, B.S. Clausen, J. Catal. 240 (2006) 108.
[33] I.C. Oppenheim, D.J. Trevor, C.E.D. Chidsey, P.L. Trevor, K. Sieradkzi, Science 254 (1991) 687.
[34] G. Hutchings, Gold Bull. 37 (2004) 3.